Dalton Transactions

PAPER

View Article Online
View Journal | View Issue

Cite this: *Dalton Trans.*, 2019, **48**, 17887

Accelerating ethylene polymerization using secondary metal ions in tetrahydrofuran†

Dawei Xiao, Zhongzheng Cai and Loi H. Do *

Received 5th November 2019,
Accepted 21st November 2019

DOI: 10.1039/c9dt04288a

rsc.li/dalton

We have prepared a new series of nickel phosphine phosphonate ester complexes that feature two metal-chelating polyethylene glycol (PEG) side arms. Metal binding and reactivity studies in polar solvents showed that they readily coordinate external cations, including alkali (Li^+, Na^+, K^+), alkaline (Mg^{2+}, Ca^{2+}), transition (Sc^{3+}, Co^{2+}, Zn^{2+}), post-transition (Ga^{3+}), and lanthanide (La^{3+}) metals. Although olefin polymerization reactions are typically performed in non-polar solvents, which cannot solubilize +2 and +3 metal cations, we discovered that our nickel catalysts could promote ethylene polymerization in neat tetrahydrofuran. This advance allowed us, for the first time, to systematically investigate the effects of a wide range of M^+, M^{2+}, and M^{3+} ions on the reactivity of nickel olefin polymerization catalysts. In ethylene homopolymerization, the addition of $Co(OTf)_2$ to our nickel-PEG complexes provided the largest boost in activity (up to 11-fold, 2.7×10^6 g mol^{-1} h^{-1}) compared to that in the absence of external salts. The catalyst enhancing effects of secondary metals were also observed in studies of ethylene and polar olefin (*e.g.*, propyl vinyl ether, allyl butyl ether, methyl-10-undecenoate, and 5-acetoxy-1-pentene) copolymerization. Notably, combining either Co^{2+} or Zn^{2+} with our nickel complexes increased the rates of polymerization in the presence of propyl vinyl ether by about 5.0- and 2.4-fold, respectively. Although further studies are needed to elucidate the structural and mechanistic roles of the secondary metals, this work is an important advance toward the development of cation-switchable polymerization catalysts.

Introduction

Although polyolefins have been produced commercially since the 1930s,[1] achieving high precision in the polymerization process is still an ongoing challenge.[2–4] Advances in late transition metal catalysis have led to the development of a diverse assortment of nickel and palladium complexes that are capable of polymerizing both non-polar and polar olefins.[5–9] However, because the coordination insertion process is complex, controlling how each olefin is incorporated and the total number of monomers in each polymer chain is difficult to achieve. Many creative strategies have been employed to obtain polyolefins with unique microstructures and compositions, such as the application of electronic and steric tuning,[10–13] hemi-labile ligands,[14,15] or bimetallic active sites.[16,17] Given the ever growing demand for new materials with new properties, there are numerous opportunities to improve upon existing polymerization technologies.[18]

To help streamline polyolefin synthesis, we are developing switchable catalysts[19] that could be easily fine-tuned by interchanging their secondary metal ions (Scheme 1).[20–23] Unlike redox switches that typically toggle between 2–3 different modes,[24–26] cation switches could access virtually unlimited number of reactivity states since their differences in properties (*e.g.*, charge, size, Lewis acidity, redox behavior, coordination geometry, *etc.*) could be exploited to alter catalysts in distinct ways. One of the earliest examples of using secondary metals to boost catalyst performance was work reported by Johnson, Brookhart, and coworkers.[27] The researchers showed that nickel catalysts in the presence of Li^+ were significantly more active in ethylene and hexyl acrylate copolymerization than in

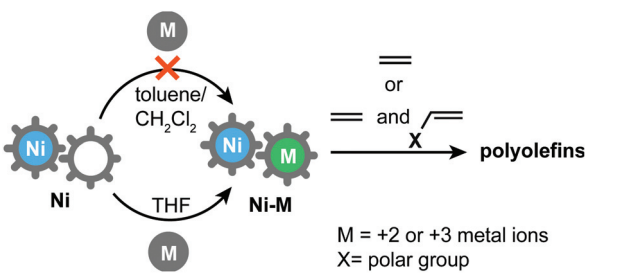

Scheme 1 Expanding the scope of secondary metal ions.

Department of Chemistry, University of Houston, 4800 Calhoun Rd., Houston, Texas, 77004, USA. E-mail: loido@uh.edu

†Electronic supplementary information (ESI) available. CCDC 1943648–1943650. For ESI and crystallographic data in CIF or other electronic format see DOI: 10.1039/c9dt04288a

its absence. Recently, Jordan and coworkers demonstrated that secondary metals such as Li^+ or Zn^{2+} could induce the self-assembly of palladium cages that are capable of polymerizing ethylene to high molecular weight polymers.[28,29] Tonk's research group has studied nickel–zinc heterobimetallics (**Ni1**–Zn[30] and **Ni2**–Zn,[31] Chart 1) and showed that they exhibit distinct reactivity from that of mononickel complexes that lack zinc. Our research group's efforts to create cation-responsive catalysts have led to the development of nickel phenoxyimine (**Ni3**),[32,33] nickel phenoxyphosphine (**Ni4**),[34] and palladium phosphine phosphonate ester (**Pd1**)[35] complexes bearing polyethylene glycol (PEG) chelators for binding external metal ions (Chart 1). We established through both solution and X-ray crystallographic studies that these complexes readily formed 1 : 1 nickel–alkali or palladium–alkali species. In general, we observed that addition of alkali salts to the catalysts often led to significant polymerization rate enhancements and changes in their polymer molecular weight and branching. Unlike in systems that utilize boranes as remote Lewis acid activators,[36,37] the secondary metals in our catalysts could be easily removed (*e.g.*, by the addition of crown ethers). Our PEGylated complexes are also amenable to conventional electronic and steric modifications, which means that many degrees of tuning are possible to optimize the catalysts.[33]

Although we successfully demonstrated the beneficial effects of secondary metal ions on polymerization,[32–35] our previous studies were limited to alkali (Li^+, Na^+, and K^+) tetraaryl borate salts because they could be readily dissolved in typical polymerization solvents, such as toluene, xylene, trichlorobenzene, and dichloromethane. Because most +2, +3, and higher charged cations are not soluble in hydrocarbon or halogenated solvents, we could not incorporate non-alkali ions into our catalysts (Scheme 1). In the present work, we have overcome this solubility problem by developing nickel phosphine phosphonate-PEG complexes that are active in tetrahydrofuran (THF).[38,39] This advance enabled us to broaden the scope of secondary metals to study, including alkaline, transition, post-transition, and lanthanide ions. Interestingly, we discovered that out of a select group of metal salts tested, Zn^{2+} and Co^{2+} provided the greatest catalyst enhancements in both ethylene homopolymerization and ethylene and polar olefin copolymerization. These results suggest that cation-switchable catalysis could be a viable approach toward synthesizing different designer polyolefins from a general catalyst platform. We will discuss how these studies have informed our ongoing catalyst design efforts and the challenges to be addressed in future work.

Results and discussion

Synthesis of P,O-ligands and their nickel complexes

Our previous success in using phosphine phosphonate-PEG ligands to prepare palladium catalysts led us to use this platform for nickel.[35,40] The ligands **3a** (Ar = 2-methoxyphenyl) and **3b** (Ar = 2,6-dimethoxyphenyl) were synthesized according to our standard procedures (see Experimental section). The P,O-ligands were metallated by mixing with $AgSbF_6$ and $[Ni(allyl)(Cl)]_2$ to furnish either **4a** or **4b** (Scheme 2).

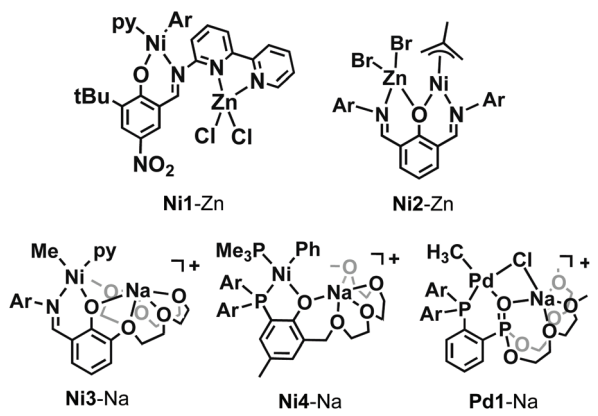

Chart 1 Crystallographically characterized heterobimetallic complexes (**Ni1**–Zn, **Ni2**–Zn, **Ni3**–Na, **Ni4**–Na, and **Pd1**–Na) studied for their olefin polymerization activity.

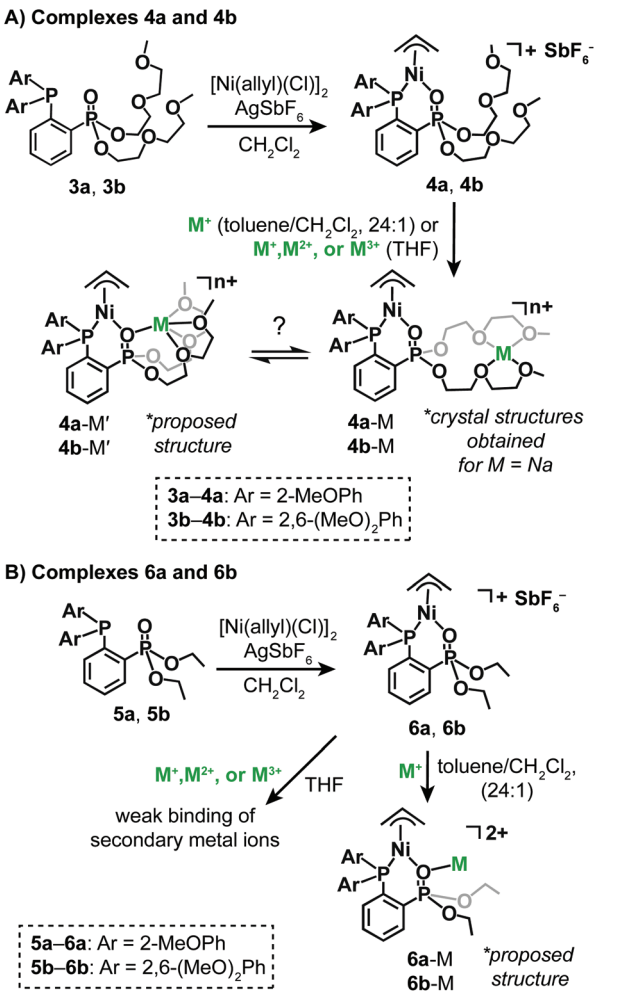

Scheme 2 Synthesis of the nickel complexes and metallation with M^{n+} ions. Metal ions studied in this work: Li^+, Na^+, K^+, Mg^{2+}, Ca^{2+}, Co^{2+}, Cu^{2+}, Zn^{2+}, Sn^{2+}, Al^{3+}, Sc^{3+}, Ga^{3+}, Bi^{3+}, and La^{3+}.

Compound **4a** was isolated as a dark red oil whereas **4b** was an orange solid. As standard catalysts, we also synthesized complexes **6a** and **6b** that have ethoxy instead of PEG groups. The X-ray crystal structure of **6a** (Fig. S56†) indicates that the nickel center is ligated by both P- and O-donors from the phosphine phosphonate ester ligand (Ni–P = 2.20 Å and Ni–O = 1.92 Å) and has an allyl group bound in an η^3 coordination mode.

Secondary metal ion binding

Similar to their palladium analogues,[35] our nickel complexes readily formed adducts with $LiBAr^F{}_4$, $NaBAr^F{}_4$, and $KBAr^F{}_4$ ($BAr^F{}_4{}^-$ = tetrakis(3,5-bis(trifluoromethyl)phenyl)borate anion) in non-polar solvents. The nickel–alkali binding behavior was studied by ^{1}H NMR spectroscopy in $CDCl_3$. We observed that the resonance for the allyl hydrogen atom at ~5.7 ppm for both **4a** (Fig. S1†) and **4b** (Fig. S2–S4) shifted upfield upon the addition of alkali salts. Job plot[41] analysis of the NMR data for **4a** + Na^+ and **4b** + Na^+ suggests that the optimal nickel : sodium binding stoichiometry is 1 : 1 (Fig. 1, peak maxima at χ_{Ni} = 0.5). Interestingly, the ^{31}P NMR spectra of **4a** *vs.* **4a**/Na^+ (Fig. S9†) and **4b** *vs.* **4b**/Na^+ (Fig. S10†) in $CDCl_3$ showed peaks with nearly identical chemical shifts, suggesting that the sodium ions do not interact directly with the phosphine oxide moiety. Solution binding studies conducted in THF instead of $CDCl_3$ showed NMR spectral shifts of the allyl group when either Na^+ or Zn^{2+} was added to **4a** at 40–50 °C (Fig. S6–S8). Unfortunately, we do not currently understand why the peak shifts are temperature dependent.

To determine the structures of the nickel–sodium species in the solid state, single crystals were grown by slow diffusion of pentane into a THF/Et_2O mixture containing the nickel complexes and $NaSbF_6$ (1 : 1) (crystals could not be grown using $NaBAr^F{}_4$). X-ray diffraction analysis of the **4a** + Na^+ crystals showed a complex with the formulation [NiNa(allyl)(**3a**)$(SbF_6)_2$] (**4a**-Na, Fig. 2). The nickel center has the expected distorted planar geometry with Ni–P and Ni–O bond distances of 2.19 and 1.92 Å, respectively, similar to those in mononickel **6a** (Fig. S56†). Additionally, four oxygen donors from the pendent PEG chains (Na–O bond distances range from 2.40 to 3.00 Å) and two fluorine donors from two SbF_6^- anions (Na–F = ~2.30 Å) occupy the sodium coordination sphere. Surprisingly, the phosphonate oxygen donor does not coordinate to Na^+ and the nickel–sodium separation is ~6.68 Å, which is much longer than those in our other heterobimetallic structures (Chart 1).[32,34,35] The X-ray structure of **4b** + Na^+ revealed a discrete complex with the composition [NiNa(allyl)(**3b**)(SbF_6)]SbF_6 (**4b**-Na, Fig. S55†). The structure of **4b**-Na is similar to that of **4a**-Na, except that one of the methoxy groups in **4b**-Na appears to have close contact with its nickel center ($Ni–O_{methoxy}$ = 2.61 Å, van der Waals distance is ~3.55 Å[42]). Interestingly, the phosphonate oxygen donor also does not interact with Na^+, which is consistent with our ^{31}P NMR data (Fig. S9 and S10).

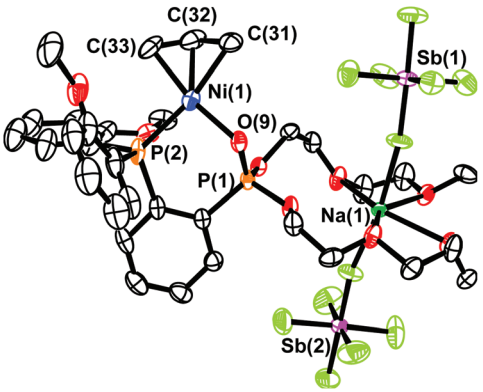

Fig. 2 X-ray crystal structure of complex **4a**-Na (ORTEP view, displacement ellipsoids drawn at 30% probability level). Hydrogen atoms and disordered THF/pentane molecules have been omitted for clarity.

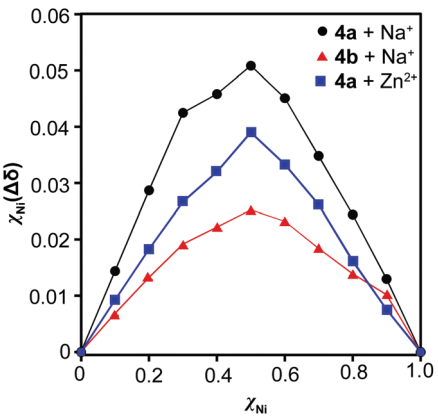

Fig. 1 Job plots for the nickel complexes with $NaBAr^F{}_4$ (**4a** + Na^+ = black dots, **4b** + Na^+ = red triangles) in $CDCl_3$ or $Zn(OTf)_2$ (**4a** + Zn^{2+} = blue squares) in CD_3CN. The mole fraction χ_{Ni} = [nickel]/([nickel] + [M^{n+}]). The total concentration of nickel and secondary metal salts is 6 mM for all data points. The Job plot data for **4b** + Li^+ and **4b** + K^+ are given in Tables S3 and S4,† respectively; they also show 1 : 1 binding.

Solution studies were then performed to investigate whether non-alkali metal ions could coordinate to the nickel phosphine phosphonate-PEG complexes. When 1 equiv. of $Co(OTf)_2$ (OTf^- = $SO_3CF_3^-$ triflate anion) was added to **4a** in CD_3CN, the NMR peaks became significantly broadened due to the paramagnetism of Co^{2+} (Fig. S11†). Interaction of Co^{2+} with **4a** was further established by UV-vis absorption spectroscopy, which showed a bathochromic shift of the band at ~400 nm to ~410 nm and increase in peak intensity upon the addition of excess $Co(OTf)_2$ to a THF solution of the nickel complex (Fig. S12†). These spectral changes suggest that cobalt is capable of binding **4a** but the exact structure of the **4a**-Co complex is uncertain.

When diamagnetic $Zn(OTf)_2$ was combined with **4a** in CD_3CN, the allyl hydrogen peak at 5.7 ppm shifted downfield when increasing amounts of Zn^{2+} were introduced (Fig. S5†). The Job plot obtained from mixing **4a** + Zn^{2+} in different ratios suggests that the **4a**-Zn complex has a 1 : 1 nickel : zinc stoichiometry (Fig. 1, blue squares). Unfortunately, despite many attempts to grow single crystals of either **4a**-Co or **4a**-Zn for

X-ray structural characterization, our efforts were not successful.

As shown in Scheme 2A, we propose that the heterobimetallic species above could adopt one of two structural motifs, either an open (**4a**-M or **4b**-M) or bridged (**4a**-M′ or **4b**-M′) form. It is also feasible that the two structural isomers could exist in equilibrium. Although we have only obtained structures of the open form for nickel (*e.g.*, **4a**-Na in Fig. 2 and **4b**-Na in Fig. S55†), our previous studies showed that the phosphine phosphonate-PEG ligands could bridge two different metal ions in the presence of chloride (*e.g.*, **Pd1**–Na, Chart 1). However, it is possible that in the absence of suitable external bridge anions, **4a**-M/**4b**-M may be preferred over **4a**-M′/**4b**-M′.

For comparison, we next investigated the metal binding behavior of the conventional complex **6a**, which lacks the two PEG chains present in **4a** and **4b**. In the non-coordinating solvent $CDCl_3$, the addition of 1 equiv. of $NaBAr^F{}_4$ to **6a** led to subtle but distinct changes to its ^1H NMR spectrum (Fig. S13†). For example, the allyl hydrogen peak at 5.72 ppm shifted upfield to 5.65 ppm in the presence of Na^+. These changes are most likely due to binding of Na^+ to one or more of the oxygen donors in the phosphonate ester group of **6a**. Interestingly, when 1 equiv. of $Zn(OTf)_2$ was added to **6a** in CD_3CN, many additional NMR peaks appeared (Fig. S14†), suggesting that more than one new species had formed. Since **6a** does not have a well-defined pocket for secondary metals, Zn^{2+} could bind **6a** at multiple sites. As demonstrated by our polymerization results below, there appears to be a strong correlation between the stability of the nickel–metal complexes and their catalyst activity (Fig. 3).

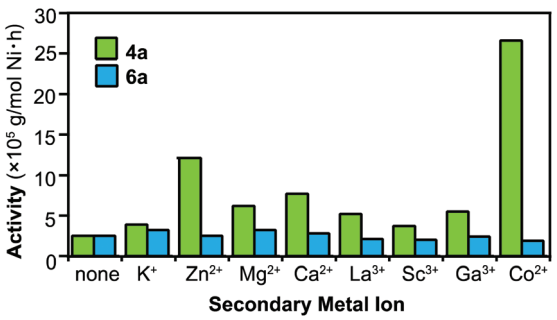

Fig. 3 Comparison of catalyst activity in ethylene homopolymerization using either **4a** or **6a** in the presence of various metal triflate salts (THF solvent). See Table S8† for detailed polymerization data.

Ethylene homopolymerization studies in toluene and dichloromethane

To determine whether our nickel complexes are competent catalysts, they were first tested in ethylene homopolymerization. For these studies, the Ni complexes were dissolved in a mixture of toluene and dichloromethane (24 : 1) and then stirred under ethylene (200 or 400 psi) at 80 °C for 1 h (Table 1). In general, all of the catalysts exhibited moderate activity (~10^5 g mol^{-1} h^{-1}) and gave polyethylene (PE) with moderate branching (13–22 per 1000 carbons) and low molecular weight (M_n = ~10^2 to 10^3). Consistent with established trends,[10,43] the bulkier catalysts **4b** (entry 3) and **6b** (entry 7) were less active but provided PE with higher M_n than their corresponding less bulky **4a** (entry 1) and **6a** (entry 5) complexes, respectively. These data also indicated that the PEG groups in **4a** and **4b** are not catalyst inhibiting since their non-PEGylated counterparts gave similar results. All of the PE produced showed relatively narrow polydispersity (M_w/M_n typically less than 2.0), suggesting that the nickel complexes are single component catalysts.

Next, we evaluated the effects of adding alkali salts to the polymerization reactions in toluene/dichloromethane (24 : 1) (Tables 1 and S6†). For the catalysts containing 2-methoxyphenyl substituents (*i.e.*, **4a** and **6a**), the presence of 1 equiv. of $LiBAr^F{}_4$, $NaBAr^F{}_4$, or $KBAr^F{}_4$ relative to nickel, resulted in up to ~3.5-fold increase in catalyst activity. Interestingly, the PE products had similar morphologies regardless of whether alkali salts were used. The activity enhancing effects of M^+ is tentatively attributed to electrophilic activation and/or greater structural stability (*vide infra*).[34,35] The addition of alkali ions to the bulkier catalysts **4b** and **6b**, led to slight decreases in polymerization rates. Because these catalysts bear sterically demanding 2,6-dimethoxyphenyl substituents, the binding of alkali ions to either **4b** or **6b** may cause excessive steric congestion at the active site, thereby reducing polymerization efficiency.

Table 1 Ethylene homopolymerization data for **4a**, **4b**, **6a**, and **6b**[a]

Entry	Complex	Salt	Polymer yield (g)	Activity (×10^5 g mol^{-1} h^{-1})	Branches[c] (/1000 C)	M_n [d] (×10^3)	M_w/M_n [d]
1	**4a**	None	8.6	8.6	22	0.84	1.7
2	**4a**	Na^+	29.9	29.9	30	1.04	1.2
3[b]	**4b**	None	6.1	3.0	13	4.79	1.4
4[b]	**4b**	Na^+	3.5	1.8	16	7.61	1.4
5	**6a**	None	7.4	7.4	18	0.69	1.7
6	**6a**	Na^+	26.6	26.6	26	0.98	2.0
7[b]	**6b**	None	5.4	2.7	17	7.36	1.2
8[b]	**6b**	Na^+	3.3	1.6	15	13.92	1.3

[a] Polymerization conditions: Ni catalyst (10 μmol), $MBAr^F{}_4$ (10 μmol), ethylene (200 psi), 2 mL DCM, 48 mL toluene, 1 h at 80 °C. [b] Polymerization conditions: Ni catalyst (20 μmol), $MBAr^F{}_4$ (20 μmol), ethylene (400 psi), 2 mL DCM, 48 mL toluene, 1 h at 80 °C. [c] The total number of branches per 1000 carbons was determined by ^1H NMR spectroscopy. [d] Determined by GPC in trichlorobenzene at 150 °C.

Ethylene homopolymerization studies in tetrahydrofuran

To expand our studies of secondary metal ions, we first had to identify a polymerization-compatible solvent that could dissolve +2 and +3 metal salts. Li and coworkers showed that nickel phenoxyphosphine catalysts are active in the presence of 2 M polar solvent additives, such as ethanol, diethyl ether, acetone, ethyl acetate, water, acetonitrile, and dimethylformamide.[39] There are only a few reports of coordination insertion polymerizations performed in neat polar solvent, specifically in water[44–47] and THF.[38] Coordinating/polar solvents are typically avoided in polymerization reactions because they could compete with olefin binding and thus, diminish catalyst efficiency. Motivated by the studies above, we proceeded to test our nickel catalysts in the presence of varying amounts of THF in toluene. To our surprise, the polymerization data showed that the nickel catalysts were relatively tolerant of THF (Table 2). For catalyst **4a**, the use of 4% THF (entry 2) led to no loss in activity, whereas the use of 20% THF (entry 3) led to only ~1.3-fold reduction in activity compared to reactions conducted in the absence of THF (entry 1). Interestingly, complex **4a** in neat THF still gave a moderate activity of 2.5×10^5 g mol^{-1} h^{-1} (entry 4). When K^+ was added to **4a**, excellent activity was observed up to 20% THF (3.1×10^6 g mol^{-1} h^{-1}, entry 7). As expected, in 100% THF (entry 8), the activity of **4a**-K dropped about 3.8-folds compared to that in 0% THF (entry 5). Similar reactivity trends were observed for the standard catalyst **6a** in the presence and absence of alkali salts (entries 10–18).

The results above encouraged us to extend the scope of our cation studies. To survey secondary metals from different groups of the periodic table, we chose a variety of salts from the alkaline, transition, post-transition, and lanthanide metal series. Using our standard reaction conditions in neat THF, we found that adding metal halides to **4a** typically reduced (*e.g.*, Ca^{2+}, Co^{2+}) or inhibited (*e.g.*, Mg^{2+}, Al^{3+}, Fe^{3+}, Cu^{2+}) ethylene homopolymerization (Table S7†). Interestingly, the presence of zinc chloride gave a 6.8-fold increase in activity (1.7×10^6 g mol^{-1} h^{-1}) compared to that in its absence (2.5×10^5 g mol^{-1} h^{-1}). Substituting $ZnCl_2$ with either $ZnBr_2$ or ZnI_2, however, led to lower catalyst activity (~1.7×10^5 g mol^{-1} h^{-1}). It is generally observed that coordinating anions, such as halides, poison metal catalysts by occupying open coordination sites.[48] However, perhaps in the **4a**/$ZnCl_2$ complex, the chloride ions may be involved in stabilizing the active nickel–zinc species.[49] In related studies, Tonks and coworkers found that NiZn complexes featuring bridging halides showed lower ethylene polymerization activity than their mononickel counterparts (**Ni2**–Zn, Chart 1).[31] In contrast, NiZn complexes with non-bridging halides (**Ni1**–Zn) showed increased ethylene polymerization rates compared to that of their parent nickel complexes.[30] Since we were unable to obtain crystallographic characterization of **4a**/$ZnCl_2$, we are uncertain how the chloride is incorporated into our nickel–zinc structures.

To avoid the use of halides, we screened a variety of metal triflate salts instead (Table S8†). When **4a** was combined with 1 equiv. of metal triflate in THF and then exposed to 200 psi of ethylene for 1 h at 80 °C, high polymerization activity was observed for K^+, Zn^{2+}, Mg^{2+}, Ca^{2+}, La^{3+}, Sc^{3+}, Ga^{3+}, and Co^{2+} (from 3.7×10^5 to 2.7×10^6 g mol^{-1} h^{-1}, entries 2–11). Polymerization rate enhancements of 10.6- and 4.8-fold were obtained using cobalt and zinc salts, respectively, relative to that of the control. The PE products produced in all reactions were similar, with moderate branches (18 to 27 per 1000 carbons), low molecular weight (M_n = $<1 \times 10^3$), and relatively narrow polydispersity ($M_w/M_n \leq 2.1$). Surprisingly, Cu^{2+} completely shut down the activity (Table S8,† entry 12), whereas Al^{3+} (entry 13) and Bi^{3+} (entry 15) lowered the activity of **4a**.

Table 2 Ethylene homopolymerization data for **4a** and **6a** in toluene and THF solvent mixtures[a]

Entry	Complex	Salt	Amount of THF[c]	Polymer yield (g)	Activity ($\times 10^5$ g mol^{-1} h^{-1})	Branches[d] (/1000 C)	M_n[e] ($\times 10^3$)	M_w/M_n[e]
1[b]	**4a**	None	0%	8.6	8.6	22	0.84	1.7
2	**4a**	None	4%	8.7	8.7	21	1.14	1.6
3	**4a**	None	20%	6.8	6.8	19	0.86	1.3
4	**4a**	None	100%	2.5	2.5	21	0.70	1.1
5[b]	**4a**	K^+	0%	28.9	28.9	28	1.12	1.2
6	**4a**	K^+	4%	28.7	28.7	32	0.84	1.7
7	**4a**	K^+	20%	30.9	30.9	31	0.77	2.2
8	**4a**	K^+	100%	7.5	7.5	24	0.83	1.9
9	**4a**	Na^+	100%	6.1	6.1	24	0.95	1.2
10[b]	**6a**	None	0%	7.4	7.4	18	0.69	1.7
11	**6a**	None	4%	4.1	4.1	16	1.64	1.2
12	**6a**	None	20%	7.5	7.5	17	0.78	1.5
13	**6a**	None	100%	2.5	2.5	19	0.90	1.2
14[b]	**6a**	K^+	0%	25.4	25.4	22	0.73	1.7
15	**6a**	K^+	4%	21.9	21.9	24	0.87	1.6
16	**6a**	K^+	20%	36.3	36.3	27	0.61	1.6
17	**6a**	K^+	100%	6.6	6.6	21	0.95	1.2
18	**6a**	Na^+	100%	6.5	6.5	19	1.01	1.7

[a] Polymerization conditions: Ni catalyst (10 μmol), $MBAr^F_4$ (10 μmol), ethylene (200 psi), toluene and THF in different ratios, 1 h at 80 °C. [b] These reactions were performed in 2 mL DCM and 48 mL toluene. [c] The percentage of THF in Toluene. [d] The total number of branches per 1000 carbons was determined by ^{1}H NMR spectroscopy. [e] Determined by GPC in trichlorobenzene at 150 °C.

Control polymerization studies using the ligand **3a**/$Co(OTf)_2$ or complex **4a**/Ag(OTf) in the presence of 200 psi of ethylene in THF at 80 °C did not provide any polymer products. Many factors could account for differences in the secondary metal ion effects, such as the coordination preferences of the PEG chelator for M^{n+}, solubility of the metal salts in THF, and/or nickel : M^{n+} binding stoichiometry. Detailed studies to characterize the various mixed metal complexes are needed to better understand their structures and reactivity.

The important role of the PEG chains in binding secondary metals was apparent by comparing the reactivity of **4a** *vs.* **6a** in THF (Fig. 3). For example, ethylene polymerization using **6a** in combination with K^+, Zn^{2+}, Mg^{2+}, Ca^{2+}, La^{3+}, Sc^{3+}, Ga^{2+}, or Co^{2+} triflate had negligible effects on catalyst activity (Table S8,† entry 16 *vs.* entries 17–24). Since THF solvent molecules are coordinating, they are capable of competing with **6a** for binding M^{n+}. These results indicate that without additional chelators to capture M^{n+}, **6a** cannot form strong adducts with external cations in polar solvents.

Ethylene and polar olefin copolymerization studies in tetrahydrofuran

The results above were exciting because they suggested that the more active **4a**-M catalysts might be capable of catalyzing the polymerization of difficult to incorporate polar monomers, including those that could form metallocyclic intermediates. In these investigations, **4a** was mixed with 1 equiv. of a metal salt and then exposed to ethylene and a polar olefin (*e.g.*, PVE = propyl vinyl ether, ABE = allyl butyl ether, MU = methyl-10-undecenoate, AP = 5-acetoxy-1-pentene, and MA = methyl acrylate) in THF for 2 h at 80 °C (Table 3). For ethylene and PVE copolymerization, we found that **4a**-Co (entry 2) and **4a**-Zn (entry 3) showed a 5.0- and 2.4-fold boost in catalyst activity, respectively, compared to that of **4a** alone (entry 1). The poly (ethylene-*co*-PVE) products were washed with chloroform to remove any trace impurities and their identities were confirmed by ^{1}H (Fig. S44†) and ^{13}C NMR (Fig. S45†) spectroscopy. The nickel–potassium complex **4a**-K (entry 4) gave only a modest 1.1-fold increase in catalyst activity compared to that of **4a** only. As a control, reaction of ethylene and PVE in the presence of only $Co(OTf)_2$ (*i.e.*, without **4a**) did not yield any polymers (entry 5). Interestingly, copolymerization of ethylene and PVE using **6a** was not enhanced in the presence of Co^{2+} (*cf.* entries 6 *vs.* 7).

Under similar reaction conditions, **4a** itself was a poor catalyst for ethylene and ABE copolymerization (Table 3, entry 8). However, moderate activities of 1.9×10^3 and 1.0×10^3 g mol^{-1} h^{-1} were observed in the presence of Co^{2+} (entry 9) and Zn^{2+} (entry 10) ions, respectively. The polymers obtained were confirmed to be poly(ethylene-*co*-ABE) by ^{1}H NMR spectroscopy (Fig. S46†).

Examples of ethylene and vinyl or allyl ether copolymerization by late transition metal catalysts are relatively rare (Table S9†). A survey of the literature revealed that the most successful nickel-based systems are those ligated by imidazo[1,5-*a*]quinolin-9-olate-1-ylidene (**7**),[50] phosphine sulfonate (**8**,[51] **10**[52]), and diphosphazane monoxide (**9**).[53] Interestingly, our **4a**-Co complex is so far the most active nickel catalyst for ethylene and vinyl ether copolymerization. For example, **4a**-Co (activity = 3.4×10^4 g mol^{-1} h^{-1}) is about 20-fold more active than **9** (1.7×10^3 g mol^{-1} h^{-1}) under optimized conditions. However, our nickel–cobalt catalysts furnished copolymers with lower comonomer incorporation (0.2 mol% for **4a**-Co *vs.* 2.0 mol% for **9**) and slightly lower molecular weight (1.3×10^3

Table 3 Ethylene and polar olefin copolymerization data for **4a** with metal salts in THF[a]

Entry	Cat.	Salt	Comonomer[c] (conc., M)	Polymer yield (g)	Activity ($\times 10^3$ g mol^{-1} h^{-1})	Branches[d] (/1000 C)	M_n [e] ($\times 10^3$)	Inc.[f] (mol%)	M_w/M_n [e]
1	**4a**	None	PVE (1.0)	0.55	6.9	21	1.43	0.21	1.2
2	**4a**	$Co(OTf)_2$	PVE (1.0)	2.74	34.2	25	1.29	0.17	1.3
3	**4a**	$Zn(OTf)_2$	PVE (1.0)	1.34	16.8	27	1.14	0.24	1.2
4	**4a**	$KBAr^F_4$	PVE (1.0)	0.61	7.6	23	1.26	0.25	1.8
5	none	$Co(OTf)_2$	PVE (1.0)	0	—	—	—	—	—
6	**6a**	None	PVE (1.0)	0.58	7.2	18	0.74	0.17	1.5
7	**6a**	$Co(OTf)_2$	PVE (1.0)	0.47	5.8	18	0.82	0.14	1.4
8	**4a**	None	ABE (0.5)	<0.01	<0.1	—	—	—	—
9	**4a**	$Co(OTf)_2$	ABE (0.5)	0.15	1.9	23	3.35	0.21	2.4
10	**4a**	$Zn(OTf)_2$	ABE (0.5)	0.08	1.0	25	1.50	0.33	1.5
11[b]	**4a**	None	MU (0.5)	0.58	14.5	20	1.61	0.38	1.3
12[b]	**4a**	$Co(OTf)_2$	MU (0.5)	2.94	73.5	23	2.15	0.69	1.5
13[b]	**4a**	$Zn(OTf)_2$	MU (0.5)	2.44	61.0	23	1.94	0.74	1.3
14	**4a**	None	AP (0.5)	0.73	9.1	21	2.23	0.31	1.6
15	**4a**	$Co(OTf)_2$	AP (0.5)	5.45	68.1	28	1.78	0.20	1.4
16	**4a**	$Zn(OTf)_2$	AP(0.5)	2.17	27.1	21	1.82	0.29	1.2
17	**4a**	None	MA (1.0)	0	—	—	—	—	—
18	**4a**	$Co(OTf)_2$	MA (1.0)	0	—	—	—	—	—

[a] Polymerization conditions: Ni catalyst (40 μmol), metal salt (40 μmol), ethylene (400 psi), 50 mL of THF, 2 h at 80 °C. [b] Polymerization conditions: Ni catalyst (20 μmol), metal salt (20 μmol). [c] Comonomer abbreviation: PVE = propyl vinyl ether, ABE = allyl butyl ether, MU = methyl-10-undecenoate, AP = 5-acetoxy-1-pentene, MA = methyl acrylate. [d] The total number of branches per 1000 carbons was determined by ^{1}H NMR spectroscopy. [e] Determined by GPC in trichlorobenzene at 150 °C. [f] Determined by ^{1}H NMR spectroscopy.

for **4a**-Co *vs.* 8.0×10^3 for **9**). The low comonomer incorporation (<1 mol%) in our polymers suggests that not every chain contains a polar olefin. It is possible that the incorporation of polar monomers leads to chain capping/termination rather than copolymerization. On the basis of previous work,[33] we expect that increasing the steric bulk of our catalysts would increase their polymer molecular weights. In comparison to nickel, more examples are known for palladium catalysts that are capable of catalyzing ethylene and ether olefin copolymerization.[54] They include palladium complexes bearing phosphine sulfonate (**11**,[55] **13**,[56] **17**[57]), phosphine phosphine oxide (**12**,[12] **14**,[58] **16**[59]), and diimine (**15**)[60] ligands. To date, it is still challenging to obtain catalysts that are fast (activity $>10^4$ g mol^{-1} h^{-1}) and produce copolymers with high ether monomer incorporation (>2 mol%) and molecular weight ($>10^4$).

It has been demonstrated that increasing the distance between the polar group and the double bond typically leads to enhanced catalyst compatibility of polar olefins.[15,16,61] These specialized monomers cannot form stable five- and six-membered ring intermediates that are believed to inhibit the polymerization process.[62] Our studies showed that both MU and AP could be incorporated using **4a**. In the absence of external metal salts, **4a** provided poly(ethylene-*co*-MU) with about 0.38 mol% with an activity of 1.4×10^4 g mol^{-1} h^{-1} (Table 3, entry 11). When 1 equiv. of $Co(OTf)_2$ (entry 12) or $Zn(OTf)_2$ (entry 13) was added to **4a**, the activity increased by about 5.1- and 4.2-fold, respectively. The MU incorporation increased slightly with metal salts (*e.g.*, 1.8-fold for Co^{2+} and 1.9-fold for Zn^{2+}). Similarly, the addition of Co^{2+} or Zn^{2+} to **4a** also led to greater polymerization rates in the presence of AP. The presence of Co^{2+} increased activity by 7.5-fold (entry 15), whereas the presence of Zn^{2+} increased activity by 3.0-fold (entry 16).

Catalyst **4a** was found to be inactive for ethylene and methyl acrylate copolymerization (Table 3, entry 17). The addition of $Co(OTf)_2$ also had no beneficial effects (entry 18). Since polyethylene was not obtained from either reactions, we concluded that MA is catalyst inhibiting.

Fig. 4 summarizes our polymerization data for **4a**, **4a**-Co, and **4a**-Zn. Our results showed that the relative reactivity of the polar comonomers tested are in the order MU > AP > PVE > ABE ≫ MA. In almost all cases, the addition of $Co(OTf)_2$ to **4a** led to greater polymerization rate enhancements than the addition of $Zn(OTf)_2$.

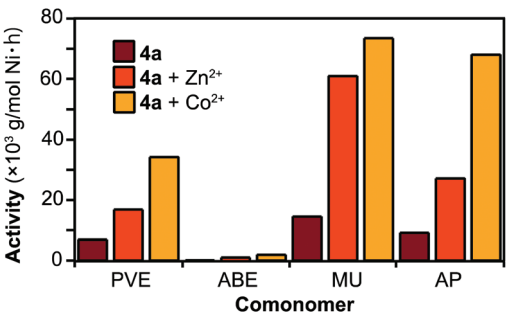

Fig. 4 Comparison of catalyst activity in ethylene and polar olefin copolymerization studies by **4a**, **4a**-Zn, and **4a**-Co. Detailed polymerization data are provided in Table 3. Abbreviations: PVE = propyl vinyl ether, ABE = allyl butyl ether, MU = methyl-10-undecenoate, AP = 5-acetoxy-1-pentene.

In reactions involving functional monomers, we discovered that solvents have minimal impact on polymerization rates. For example, when **4a** was used in the polymerization of ethylene and PVE in toluene, the activity was measured to be 6.7×10^3 g mol^{-1} h^{-1}, which is similar to that when the reaction was performed in neat THF (activity = 6.9×10^3 g mol^{-1} h^{-1}, Table 3, entry 1). These results suggest that when a monomer has greater coordinating ability than the solvent (*e.g.*, PVE > THF) and is present in large excess, it outcompetes solvent molecules for catalyst binding. Thus, we believe that polar solvents are not detrimental to the polymerization of certain functional olefins and are generally underutilized for this application.

Ongoing challenges

Although our results are intriguing from the switchable catalyst design standpoint, several important challenges remain. First, it is difficult to predict *a priori* whether a secondary metal would enhance or diminish catalyst performance. Although the majority of cations tested led to improved catalyst activity (*e.g.*, Li^+, Na^+, K^+, Mg^{2+}, Ca^{2+}, Co^{2+}, Zn^{2+}, Sc^{3+}, Ga^{3+}, and La^{3+}), several did not (*e.g.*, Cu^{2+}, Al^{3+}, Sn^{2+}, Bi^{3+}). We hypothesize that cations in the latter category either did not bind to the nickel complex or formed mixed metal species that are catalytically inactive. Furthermore, we cannot dismiss the possibility that the heterometallic species might precipitate out of solution when activated due to poor solubility. We propose that a more extensive set of secondary metals should be screened to determine whether any reactivity trends could be established. Preliminary studies comparing the ionic radius[63] (Fig. S17A†) and Lewis acidity[64] (Fig. S17B†) of the cations tested do not show any obvious correlation with polymerization activity (Table S10†). Detailed investigations of the active species, including their nuclearity and polymerization mechanisms, should be performed to understand the roles of secondary metals in catalysis.

Second, designing ligands that provide pre-organized heterobimetallic structures and have broad secondary metal ion specificity is difficult to achieve. Although we wanted to assemble bridged **4a**-M′ complexes to promote metal–metal cooperativity,[65] the X-ray structures of **4a**-Na and **4a**-Na indicated that they could adopt non-bridged motifs (Scheme 2A). Since the two metals do not interact in these structures, the sodium ion does not influence the electronic environment of nickel. Perhaps the lack of metal–metal cooperativity explains why the addition of cations do not affect the microstructures of our polymers, unlike in our other systems.[32] We believe that this problem could be solved by making the PEG chains more rigid so that the nickel–metal distances are shorter. To enhance the binding affinity of external cations, it might be necessary to replace PEG with other chelators that have greater metal ion specificity.

Third, despite demonstrating that our cation-switchable catalysts are capable of promoting ethylene polymerization in the presence of polar olefins (Table 3), their catalyst activities are still several orders of magnitude lower than those in ethylene homopolymerization (Tables 1 and S6†). The molecular weights of the polar copolymers also tend to be lower than those for homopolyethylene. These longstanding copolymerization problems have been attributed to stronger preferences for σ- rather than π-monomer binding, tendency to undergo β-X elimination (where X = usually acetate or halide), and backchelation by polar groups.[62] We propose that through further catalyst engineering using our site-differentiated ligands,[65] it might be possible to circumvent these undesired reaction pathways.

Conclusion

In summary, we have developed a new class of cation-responsive nickel catalysts that are active in neat tetrahydrofuran. For the first time, we were able to systematically evaluate and compare the effects of M^+, M^{2+}, and M^{3+} secondary metals on ethylene homo- and copolymerization. We discovered that a variety of alkali, alkaline, transition, post-transition, and lanthanide ions are capable of activating our nickel catalysts, some more so than others. In general, metal triflates are preferred over their metal halide salts since coordinating anions could be catalyst inhibiting. Metal binding studies indicated that Na^+ and Zn^{2+} both bind to **4a**/**4b** to form 1 : 1 species in solution. The structures of the heterobimetallic **4a**-Na and **4b**-Na complexes were determined by X-ray crystallography, which showed that the nickel and sodium ions adopt open rather than bridged structures. Among the select group of secondary metals tested, Co^{2+} and Zn^{2+} provided the greatest catalyst activity enhancements. Most notably, the **4a**-Co and **4a**-Zn catalysts were able to significantly increase ethylene polymerization rates in the presence of polar olefin (*e.g.*, PVE, ABE, MU, and AP). However, further studies are needed to understand the secondary metal effects. We anticipate that future research will lead to greater appreciation for the capabilities of cation-switchable catalysts and offer new cost- and time-saving methods to synthesize designer polyolefins.

Experimental section

General procedures

Commercial reagents were used as received. All air- and water-sensitive manipulations were performed using standard Schlenk techniques or under a nitrogen atmosphere using a glovebox. Anhydrous solvents were obtained from an Innovative Technology solvent drying system saturated with argon. High-purity polymer grade ethylene was obtained from Matheson TriGas without further purification. The compounds (2-bromophenyl)bis(2-methoxyphenyl) phosphine[35] and $[Ni(allyl)Cl]_2$ [66] were prepared according to literature procedures.

NMR spectra were acquired using JEOL spectrometers (ECA-400, 500, and 600) and referenced using residual solvent peaks. All ^{13}C NMR spectra were proton decoupled. ^{31}P NMR spectra were referenced to phosphoric acid. For polymer characterization, ^1H NMR spectroscopy: each NMR sample contained ~20 mg of polymer in 0.5 mL of 1,1,2,2-tetrachloroethane-d_2 (TCE-d_2) and was recorded on a 500 MHz spectrometer using standard acquisition parameters at 120 °C. ^{13}C NMR spectroscopy: each NMR sample contained ~50 mg of polymer and 50 mM (8.7 mg) chromium acetylacetonate Cr $(acac)_3$ in 0.5 mL of TCE-d_2 and was recorded at 120 °C (125 MHz). The samples were acquired using a 90° pulse of 11.7 μs, a relaxation delay of 4 s, an acquisition time of 0.81 s, and inverse gated decoupling. The samples were preheated for 30 min prior to data acquisition. The carbon spectra were assigned based on the chemical shift values reported in the literature.[32] The NMR spectra of poly(ethylene-*co*-PVE),[55] poly(ethylene-*co*-ABE),[52] poly(ethylene-*co*-MU),[61] and poly(ethylene-*co*-AP)[61] matched those reported.

High-resolution mass spectra were obtained from the mass spectral facility at the University of Houston. Elemental analyses were performed by Atlantic Microlab.

Gel permeation chromatography (GPC) data were obtained using a Malvern high temperature GPC instrument equipped with refractive index, viscometer, and light scattering detectors at 150 °C with 1,2,4-trichlorobenzene, stabilized with 125 ppm BHT, as the mobile phase. A calibration curve was established using polystyrene standards in triple detection mode. All molecular weights reported are based on triple detection.

Synthesis

Preparation of 4a. Inside the glovebox, a solution containing **3a** (200 mg, 0.33 mmol, 1.0 equiv.) and $AgSbF_6$ (113 mg, 0.33 mmol, 1.0 equiv.) in 10 mL of CH_2Cl_2 was stirred for 10 min at RT. Solid $[Ni(allyl)Cl]_2$ (45 mg, 0.16 mmol, 0.5 equiv.) was added in small portions. The reaction mixture was stirred for an additional 3 h. The resulting red mixture was filtered through a pipet plug and then dried under vacuum to give a dark red oil. The product was recrystallized by dissolving in CH_2Cl_2 and then layering with pentane to afford the final product as a dark red oil (289 mg, 0.31 mmol, 93.2%). ^1H NMR ($CDCl_3$, 400 MHz): δ (ppm) = 7.69 (m, 1H), 7.66 (m, 1H), 7.56 (m, 3H), 7.14–7.08 (m, 3H), 6.97 (t, J_{HH} = 7.8 Hz, 2H), 6.78 (m, 2H), 5.71 (m, 1H), 4.05 (m, 2H), 3.99 (m, 2H), 3.87 (s, 6H), 3.52 (m, 12H), 2.59 (br, 1H). ^{13}C NMR ($CDCl_3$, 125 MHz): δ (ppm) = 160.73 (d, J_{PC} = 7.4 Hz), 134.87 (dd, J_{PC} = 35.5, 13.5 Hz), 134.55, 134.44 (d, J_{PC} = 4.9 Hz), 134.12, 133.74 (t, J_{PC} = 14.8 Hz), 133.55, 131.09 (d, J_{PC} = 13.5 Hz), 127.72 (dd, J_{PC} = 188.5, 17.1 Hz), 121.75 (d, J_{PC} = 8.6 Hz), 115.62, 115.24, 114.66, 111.71 (d, J_{PC} = 4.9 Hz), 71.79, 70.35, 69.36 (d, J_{PC} = 6.1 Hz), 67.58 (d, J_{PC} = 6.1 Hz), 59.08, 56.06. ^{31}P NMR ($CDCl_3$, 162 MHz): δ (ppm) = 23.25 (d, J_{PP} = 20.4 Hz), −1.97 (d, J_{PP} = 20.6 Hz).

Preparation of 4b. Inside the glovebox, a solution containing **3b** (100 mg, 0.15 mmol, 1.0 equiv.) and $AgSbF_6$ (52 mg, 0.15 mmol, 1.0 equiv.) in 10 mL of CH_2Cl_2 was stirred for 10 min at RT. Solid $[Ni(allyl)Cl]_2$ (20 mg, 0.08 mmol, 0.5

equiv.) was added in small portions. The reaction mixture was stirred for an additional 3 h. The resulting red mixture was filtered through a pipet plug and then dried under vacuum to give a dark red oil. Upon the addition of pentane and after stirring for ~5 min, an orange solid formed. The product was recrystallized by dissolving in CH_2Cl_2 and then layering with pentane to afford the final product as orange crystals (142 mg, 0.14 mmol, 94.5%). ^{1}H NMR ($CDCl_3$, 400 MHz): δ (ppm) = 7.79 (m, 1H), 7.57 (m, 1H), 7.49 (m, 2H), 7.44 (t, J_{HH} = 8.4 Hz, 2H), 6.60 (dd, J_{HH} = 8.2, 4.0 Hz, 4H), 5.66 (m, 1H), 3.95 (m, 2H), 3.84 (m, 2H), 3.64 (s, 12H), 3.50 (m, 12H), 3.35 (s, 6H), 2.86 (br, 2H), 2.30 (d, J_{HH} = 13.2 Hz, 2H). ^{13}C NMR ($CDCl_3$, 125 MHz): δ (ppm) = 161.53 (d, J_{PC} = 2.9 Hz), 138.11 (dd, J_{PC} = 40.4, 12.7 Hz), 134.46 (d, J_{PC} = 14.6 Hz), 133.78, 133.38 (t, J_{PC} = 8.8 Hz), 131.42 (d, J_{PC} = 3.9 Hz), 129.59 (d, J_{PC} = 13.6 Hz), 124.91 (dd, J_{PC} = 184.9, 19.5 Hz), 111.86, 105.62, 105.13, 104.57 (d, J_{PC} = 3.9 Hz), 71.84, 70.40, 69.37 (d, J_{PC} = 6.9 Hz), 67.01 (d, J_{PC} = 5.8 Hz), 59.08, 55.98. ^{31}P NMR ($CDCl_3$, 162 MHz): δ (ppm) = 23.58 (d, J_{PP} = 25.9 Hz), −21.78 (d, J_{PP} = 24.1 Hz). Anal. Calc. for $C_{35}H_{49}F_6O_{11}P_2SbNi{\cdot}(CH_2Cl_2)_{0.25}$: C, 41.37; H, 4.88. Found: C, 41.30; H, 4.95.

Preparation of 6a. Inside the glovebox, a solution containing **5a** (100 mg, 0.22 mmol, 1.0 equiv.) and $AgSbF_6$ (75 mg, 0.22 mmol, 1.0 equiv.) in 10 mL of CH_2Cl_2 was stirred for 10 min at RT. Solid [Ni(allyl)Cl]$_2$ (30 mg, 0.11 mmol, 0.5 equiv.) was added in small portions. The reaction mixture was stirred for an additional 3 h. The resulting red mixture was filtered through a pipet plug and then dried under vacuum to give a dark red oil. Upon the addition of pentane and after stirring for ~5 min, a yellow solid formed. The product was recrystallized by dissolving in CH_2Cl_2 and then layering with pentane to afford the final product as yellow crystals (160 mg, 0.20 mmol, 91.6%). ^{1}H NMR ($CDCl_3$, 400 MHz): δ (ppm) = 7.85 (m, 1H), 7.69 (m, 1H), 7.58 (m, 3H), 7.14–7.08 (m, 3H), 6.98 (t, J_{HH} = 7.2 Hz, 2H), 6.79 (m, 2H), 5.72 (m, 1H), 3.97 (m, 4H), 3.88 (s, 6H), 2.55 (br, 1H), 1.18 (t, J_{HH} = 6.8 Hz, 6H). ^{13}C NMR ($CDCl_3$, 100 MHz): δ (ppm) = 160.72 (d, J_{PC} = 6.8 Hz), 135.08 (dd, J_{PC} = 36.0, 12.6 Hz), 134.64 (d, J_{PC} = 4.9 Hz), 134.11, 134.02, 133.88 (t, J_{PC} = 7.8 Hz), 133.55 (dd, J_{PC} = 5.8, 2.9 Hz), 131.17 (d, J_{PC} = 13.7 Hz), 127.85 (dd, J_{PC} = 185.8, 17.6 Hz), 121.72 (d, J_{PC} = 8.8 Hz), 115.68, 115.19, 114.56, 111.69 (d, J_{PC} = 3.9 Hz), 65.20 (d, J_{PC} = 6.8 Hz), 56.05, 15.91 (d, J_{PC} = 6.8 Hz). ^{31}P NMR ($CDCl_3$, 162 MHz): δ (ppm) = 22.91 (d, J_{PP} = 21.1 Hz), −2.33 (d, J_{PP} = 20.6 Hz). Anal. Calc. for $C_{27}H_{33}F_6O_5P_2SbNi$: C, 40.85; H, 4.19. Found: C, 40.60; H, 4.43.

Preparation of 6b. Inside the glovebox, a solution containing **5b** (100 mg, 0.19 mmol, 1.0 equiv.) and $AgSbF_6$ (66 mg, 0.19 mmol, 1.0 equiv.) in 10 mL of CH_2Cl_2 was stirred for 10 min at RT. Solid [Ni(allyl)Cl]$_2$ (26 mg, 0.10 mmol, 0.5 equiv.) was added in small portions. The reaction mixture was stirred for an additional 3 h. The resulting red mixture was filtered through a pipet plug and then dried under vacuum to give a dark red oil. Upon the addition of pentane and after stirring for ~5 min, an orange solid formed. The product was recrystallized by dissolving in CH_2Cl_2 and then layering with pentane to afford the final product as orange crystals (139 mg, 0.16 mmol, 85.9%). ^{1}H NMR ($CDCl_3$, 400 MHz): δ (ppm) = 7.66 (m, 1H), 7.58 (m, 1H), 7.51 (m, 2H), 7.44 (t, J_{HH} = 8.4 Hz, 2H), 6.61 (dd, J_{HH} = 8.2, 4.4 Hz, 4H), 5.67 (m, 1H), 3.83(m, 4H), 3.64 (s, 12H), 2.86 (br, 2H), 2.30 (d, J_{HH} = 13.2 Hz, 2H), 1.16 (t, J_{HH} = 6.8 Hz, 6H). ^{13}C NMR ($CDCl_3$, 100 MHz): δ (ppm) = 161.54 (d, J_{PC} = 2.0 Hz), 138.16 (dd, J_{PC} = 40.4, 12.7 Hz), 134.65 (d, J_{PC} = 13.6 Hz), 133.79, 132.72 (t, J_{PC} = 8.8 Hz), 131.31 (d, J_{PC} = 2.9 Hz), 129.63 (d, J_{PC} = 14.6 Hz), 125.43 (dd, J_{PC} = 181.9, 19.4 Hz), 111.78, 105.58, 105.10, 104.56 (d, J_{PC} = 2.9 Hz), 64.61 (d, J_{PC} = 6.8 Hz), 55.95, 15.88 (d, J_{PC} = 6.8 Hz). ^{31}P NMR ($CDCl_3$, 162 MHz): δ (ppm) = 23.13 (d, J_{PP} = 24.6 Hz), −21.86 (d, J_{PP} = 24.6 Hz). Anal. Calc. for $C_{29}H_{37}F_6O_7P_2SbNi$: C, 40.79; H, 4.37. Found: C, 37.98; H, 4.39. **Similar elemental analysis results were obtained from independently prepared samples. Trace impurities that do not show by NMR spectroscopy may be present.*

Metal binding studies with alkali ions

The method of continuous variation (Job plot analysis) was used to determine the binding stoichiometry of our nickel complexes with alkali ions. To perform these experiments, stock solutions of **4a** (or **4b**) (6 mM, 6 mL) and $MBAr^F{}_4$ (6 mM, 15 equiv. Et_2O to solubilize the salts, 6 mL, M = Li^+, Na^+, or K^+) were prepared separately in $CDCl_3$. Various amounts of each stock solution were added to an NMR tube so that a total volume of 1 mL was obtained. Ten different NMR samples were prepared, each containing a different ratio of **4a** (or **4b**) : M. The samples were recorded at room temperature by ^{1}H NMR spectroscopy. The hydrogen resonances centered at ~5.7 ppm corresponding to the allyl group in **4a** or **4b** shift in the presence of alkali ions. The changes in the ^{1}H NMR signals of H_a as a function of the mole fraction of the nickel complexes are provided in Tables S1–S4.†

Metal binding studies with zinc triflate

The method of continuous variation (Job plot analysis) was used to determine the binding stoichiometry of our nickel complexes with zinc ions. To perform these experiments, stock solutions of **4a** (6 mM, 6 mL) and $Zn(OTf)_2$ (6 mM, 6 mL) were prepared separately in CD_3CN. Various amounts of each stock solution were added to an NMR tube so that a total volume of 1 mL was obtained. Ten different NMR samples were prepared, each containing a different ratio of **4a** : Zn. The hydrogen resonance centered at ~5.7 ppm corresponding to the allyl group in **4a** shift in the presence of zinc ions. The changes in the ^{1}H NMR signals of H_a as a function of the mole fraction of **4a** are provided in Tables S5.†

General ethylene polymerization

Inside the glovebox, the nickel complexes (10 μmol) and alkali salts (10 μmol) were dissolved in 10 mL of toluene/DCM (8 : 2) and stirred for 10 min. By visual inspection, the resulting nickel–alkali complexes appeared to be soluble in the reaction mixture. The mixture was sealed inside a vial using a rubber septum and brought outside of the glovebox. Under an atmosphere of N_2, the catalyst solution was loaded into a syringe. To prepare the polymerization reactor, 40 mL of dry toluene

was added to an empty autoclave and preheated to the desired temperature. The autoclave was purged with ethylene (20 psi) for 1 min and then the catalyst solution was injected into the autoclave *via* syringe. The reactor pressure was increased to 200 psi of ethylene and the contents were stirred vigorously for 1 h. To stop the polymerization, the autoclave was vented and cooled in an ice bath. A solution of MeOH (100–200 mL) was added to precipitate the polymer. The polymer was collected by vacuum filtration, rinsed with MeOH, and then dried under vacuum at 80 °C overnight. The reported yields are average values of triplicate runs.

Ethylene and polar monomer copolymerization

Inside the glovebox, the nickel complexes (40 μmol) and metal triflate (40 μmol) were dissolved in 10 mL of THF and stirred for 10 min. The mixture was sealed inside a vial using a rubber septum and brought outside of the drybox. To prepare the polymerization reactor, 35–37 mL of dry THF was added to an empty autoclave and preheated to the desired temperature. The autoclave was purged with ethylene (20 psi) for 1 min and then the polar comonomer was added first, followed by injection of the catalyst solution into the autoclave *via* syringe. The reactor pressure was increased to 400 psi of ethylene and the contents were stirred vigorously for 2 h. To stop the polymerization, the autoclave was vented and cooled in an ice bath. A solution of MeOH (100–200 mL) was added to precipitate the polymer. The polymer was collected by vacuum filtration, rinsed with MeOH, and then dried under vacuum at 80 °C overnight. The poly(ethylene-*co*-PVE) products were also washed with chloroform to remove any trace monomers or poly(PVE) from the sample before characterization by GPC and NMR spectroscopy. The reported yields are average values of triplicate runs.

Conflicts of interest

There are no conflicts to declare.

Acknowledgements

We are grateful to the Welch Foundation (Grant No. E-1894 and the National Science Foundation (Grant No. CHE-1750411) for funding this research.

References

1 K. S. Whiteley, in *Ullmann's Encyclopedia of Industrial Chemistry*, Wiley-VCH Verlag GmbH & Co. KGaA, 2012, vol. 29.
2 H. Makio, H. Terao, A. Iwashita and T. Fujita, *Chem. Rev.*, 2011, **111**, 2363–2449.
3 *Polyolefins: 50 Years After Ziegler and Natta II*, ed. W. Kaminsky, Springer, Heidelberg, 2013.
4 F. Yang and X. Li, *J. Polym. Sci., Part A: Polym. Chem.*, 2017, **55**, 2271–2280.
5 B. P. Carrow and K. Nozaki, *Macromolecules*, 2014, **47**, 2541–2555.
6 L. Guo, W. Liu and C. Chen, *Mater. Chem. Front.*, 2017, **1**, 2487–2494.
7 C. Chen, *Nat. Rev. Chem.*, 2018, **2**, 6–14.
8 C. Tan and C. Chen, *Angew. Chem., Int. Ed.*, 2019, **58**, 7192–7200.
9 N. E. Mitchell and B. K. Long, *Polym. Int.*, 2019, **68**, 14–26.
10 Z. Chen, M. Mesgar, P. S. White, O. Daugulis and M. Brookhart, *ACS Catal.*, 2015, **5**, 631–636.
11 S. Dai, S. Zhou, W. Zhang and C. Chen, *Macromolecules*, 2016, **49**, 8855–8862.
12 W. Zhang, P. M. Waddell, M. A. Tiedemann, C. E. Padilla, J. Mei, L. Chen and B. P. Carrow, *J. Am. Chem. Soc.*, 2018, **140**, 8841–8850.
13 J. Gao, B. Yang and C. Chen, *J. Catal.*, 2019, **369**, 233–238.
14 C. J. Stephenson, J. P. McInnis, C. Chen, M. P. Weberski, Jr., A. Motta, M. Delferro and T. J. Marks, *ACS Catal.*, 2014, **4**, 999–1003.
15 D. Zhang and C. Chen, *Angew. Chem., Int. Ed.*, 2017, **56**, 14672–14676.
16 M. R. Radlauer, A. K. Buckley, L. M. Henling and T. Agapie, *J. Am. Chem. Soc.*, 2013, **135**, 3784–3787.
17 D. Takeuchi, Y. Chiba, S. Takano and K. Osakada, *Angew. Chem., Int. Ed.*, 2013, **52**, 12536–12540.
18 P. D. Hustad, *Science*, 2009, **325**, 704–707.
19 V. Blanco, D. A. Leigh and V. Marcos, *Chem. Soc. Rev.*, 2015, **44**, 5341–5370.
20 A. J. M. Miller, *Dalton Trans.*, 2017, **46**, 11987–12000.
21 T. Chantarojsiri, J. W. Ziller and J. Y. Yang, *Chem. Sci.*, 2018, **9**, 2567–2574.
22 C. Yoo, H. M. Dodge and A. J. M. Miller, *Chem. Commun.*, 2019, **55**, 5047–5059.
23 M. R. Kita and A. J. M. Miller, *J. Am. Chem. Soc.*, 2014, **136**, 14519–14529.
24 J. M. Kaiser and B. K. Long, *Coord. Chem. Rev.*, 2018, **372**, 141–152.
25 C. Chen, *ACS Catal.*, 2018, **8**, 5506–5514.
26 J. Wei and P. L. Diaconescu, *Acc. Chem. Res.*, 2019, **52**, 415–424.
27 L. Johnson, L. Wang, S. McLain, A. Bennett, K. Dobbs, E. Hauptman, A. Ionkin, S. Ittel, K. Kunitsky, W. Marshall, E. McCord, C. Radzewich, A. Rinehart, K. J. Sweetman, Y. Wang, Z. Yin and M. Brookhart, in *Beyond Metallocenes*, American Chemical Society, 2003, vol. 857, ch. 10, pp. 131–142.
28 Q. Liu and R. F. Jordan, *Organometallics*, 2018, **37**, 4664–4674.
29 Q. Liu and R. F. Jordan, *J. Am. Chem. Soc.*, 2019, **141**, 6827–6831.
30 A. J. Smith, E. D. Kalkman, Z. W. Gilbert and I. A. Tonks, *Organometallics*, 2016, **35**, 2429–2432.
31 H.-C. Chiu, A. Koley, P. L. Dunn, R. J. Hue and I. A. Tonks, *Dalton Trans.*, 2017, **46**, 5513–5517.

32 Z. Cai, D. Xiao and L. H. Do, *J. Am. Chem. Soc.*, 2015, **137**, 15501–15510.
33 Z. Cai and L. H. Do, *Organometallics*, 2017, **36**, 4691–4698.
34 T. V. Tran, Y. H. Nguyen and L. H. Do, *Polym. Chem.*, 2019, **10**, 3718–3721.
35 Z. Cai and L. H. Do, *Organometallics*, 2018, **37**, 3874–3882.
36 A. M. Johnson, N. D. Contrella, J. R. Sampson, M. Zheng and R. F. Jordan, *Organometallics*, 2017, **36**, 4990–5002.
37 Z. J. A. Komon, X. Bu and G. C. Bazan, *J. Am. Chem. Soc.*, 2000, **122**, 1830–1831.
38 P. Kenyon, M. Wörner and S. Mecking, *J. Am. Chem. Soc.*, 2018, **140**, 6685–6689.
39 Y. Zhang, H. Mu, L. Pan, X. Wang and Y. Li, *ACS Catal.*, 2018, **8**, 5963–5976.
40 N. D. Contrella, J. R. Sampson and R. F. Jordan, *Organometallics*, 2014, **33**, 3546–3555.
41 J. S. Renny, L. L. Tomasevich, E. H. Tallmadge and D. B. Collum, *Angew. Chem., Int. Ed.*, 2013, **52**, 11998–12013.
42 S. S. Batsanov, *Inorg. Mater.*, 2001, **37**, 871–885.
43 D. Zhang, E. T. Nadres, M. Brookhart and O. Daugulis, *Organometallics*, 2013, **32**, 5136–5143.
44 I. Göttker-Schnetmann, B. Korthals and S. Mecking, *J. Am. Chem. Soc.*, 2006, **128**, 7708–7709.
45 A. Held and S. Mecking, *Chem. – Eur. J.*, 2000, **6**, 4623–4629.
46 D. Zhang, D. Guironnet, I. Göttker-Schnetmann and S. Mecking, *Organometallics*, 2009, **28**, 4072–4078.
47 C. Boucher-Jacobs, B. Li, C. M. Schroeder and D. Guironnet, *Polym. Chem.*, 2019, **10**, 1988–1992.
48 D. Xiao and L. H. Do, *Organometallics*, 2018, **37**, 254–260.
49 D. Xiao and L. H. Do, *Organometallics*, 2018, **37**, 3079–3085.
50 W.-j. Tao, R. Nakano, S. Ito and K. Nozaki, *Angew. Chem., Int. Ed.*, 2016, **55**, 2835–2839.
51 M. Chen and C. Chen, *ACS Catal.*, 2017, **7**, 1308–1312.
52 J. Xia, Y. Zhang, J. Zhang and Z. Jian, *Organometallics*, 2019, **38**, 1118–1126.
53 M. Chen and C. Chen, *Angew. Chem., Int. Ed.*, 2018, **57**, 3094–3098.
54 W. Heyndrickx, G. Occhipinti, P. Bultinck and V. R. Jensen, *Organometallics*, 2012, **31**, 6022–6031.
55 S. Luo, J. Vela, G. R. Lief and R. F. Jordan, *J. Am. Chem. Soc.*, 2007, **129**, 8946–8947.
56 J. Xia, Y. Zhang, X. Hu, X. Ma, L. Cui, J. Zhang and Z. Jian, *Polym. Chem.*, 2019, **10**, 546–554.
57 Y. Ota, S. Ito, J.-i. Kuroda, Y. Okumura and K. Nozaki, *J. Am. Chem. Soc.*, 2014, **136**, 11898–11901.
58 Y. Mitsushige, H. Yasuda, B. P. Carrow, S. Ito, M. Kobayashi, T. Tayano, Y. Watanabe, Y. Okuno, S. Hayashi, J. Kuroda, Y. Okumura and K. Nozaki, *ACS Macro Lett.*, 2018, **7**, 305–311.
59 Y. Mitsushige, B. P. Carrow, S. Ito and K. Nozaki, *Chem. Sci.*, 2016, **7**, 737–744.
60 M. Li, X. Wang, Y. Luo and C. Chen, *Angew. Chem., Int. Ed.*, 2017, **56**, 11604–11609.
61 C. Hong, X. Sui, Z. Li, W. Pang and M. Chen, *Dalton Trans.*, 2018, **47**, 8264–8267.
62 W. E. Piers and S. Collins, *Compr. Organomet. Chem. III*, 2007, **1**, 141–165.
63 R. Shannon, *Acta Crystallogr., Sect. A: Cryst. Phys., Diffr., Theor. Gen. Crystallogr.*, 1976, **32**, 751–767.
64 I. Brown, *Acta Crystallogr., Sect. B: Struct. Sci.*, 1988, **44**, 545–553.
65 Z. Cai, D. Xiao and L. H. Do, *Comments Inorg. Chem.*, 2019, **39**, 27–50.
66 R. J. Hazlehurst, S. W. E. Hendriks, P. D. Boyle and J. M. Blacquiere, *ChemistrySelect*, 2017, **2**, 6732–6737.